

Multi-Epoch VLBA Observations of the Compact Wind-Collision Region in the Quadruple System Cyg OB2 #5

Sergio A. Dzib¹, Luis F. Rodríguez^{1,2}, Laurent Loinard^{1,3}, Amy J. Mioduszewski⁴, Gisela N. Ortiz-León¹ and Anabella T. Araudo¹

s.dzib@crya.unam.mx

Received _____; accepted _____

¹Centro de Radioastronomía y Astrofísica, Universidad Nacional Autónoma de México, Morelia 58089, México

²Astronomy Department, Faculty of Science, King Abdulaziz University, P.O. Box 80203, Jeddah 21589, Saudi Arabia

³Max-Planck-Institut für Radioastronomie, Auf dem Hügel 69, 53121 Bonn, Germany

⁴National Radio Astronomy Observatory, 1003 Lopezville Road, Socorro, NM 87801, USA

ABSTRACT

We present multi-epoch VLBA observations of the compact wind collision region in the Cyg OB2 #5 system. These observations confirm the arc-shaped morphology of the emission reported earlier. The total flux as a function of time is roughly constant when the source is “on”, but falls below the detection limit as the wind collision region approaches periastron in its orbit around the contact binary at the center of the system. In addition, at one of the “on” epochs, the flux drops to about a fifth of its average value. We suggest that this apparent variation could result from the inhomogeneity of the wind that hides part of the flux rather than from an intrinsic variation. We measured a trigonometrical parallax, for the most compact radio emission of 0.61 ± 0.22 mas, corresponding to a distance of $1.65^{+0.96}_{-0.44}$ kpc, in agreement with recent trigonometrical parallaxes measured for objects in the Cygnus X complex. Using constraints on the total mass of the system and orbital parameters previously reported in the literature, we obtain two independent indirect measurements of the distance to the Cyg OB2 #5 system, both consistent with 1.3–1.4 kpc. Finally, we suggest that the companion star responsible for the wind interaction, yet undetected, is of spectral type between B0.5 to O8.

Subject headings: stars: individual (Cyg OB2 #5) — stars: winds — radiation mechanisms: nonthermal — astrometry

1. Introduction

Non-thermal radio emission from a massive binary system is usually produced in the interaction of their strong winds (see De Becker 2007 for a recent review). An interesting case is the quadruple massive system Cyg OB2 #5 (V729 Cyg, BD +40 4220) that is the only multiple system known so far to harbor two radio-imaged wind-collision regions (Ortiz-León et al. 2011).

Cyg OB2 #5 is a radio-bright massive multiple system located in the Cygnus OB2 association, one of the most prominent massive young clusters known, containing over 100 O stars. The most massive component of Cyg OB2 #5 (i.e. the primary) is an eclipsing, contact binary consisting of two O-type supergiants with a 6.6-day orbital period. We shall refer to this central object as Cyg OB2 #5 A (containing the individual stars Cyg OB2 #5 Aa and Cyg OB2 #5 Ab) . Contreras et al. (1997) suggested that a radio source located $0''.8$ to the north-east of Cyg OB2 #5 A is the shock formed by the interaction between the wind from Cyg OB2 #5 A and that of a B-type star first reported by Herbig (1967) and located $0''.9$ to the north-east. We shall refer to this B star as Cyg OB2 #5 C, and to the wind-collision region between this star and Cyg OB2 #5 A as WCR(A-C). Recently, Ortiz-León et al. (2011) used the Very Long Base Array (VLBA) telescope to obtain a high angular resolution image (~ 10 mas) and reported the detection of a compact wind-collision region with possible non-thermal radio emission. This structure is formed by the interaction between the wind driven by Cyg OB2 #5 A and that of an unseen companion (that we shall call Cyg OB2 #5 B), an early B type star, with an orbital period of ~ 6.7 -yr (Kennedy et al. 2010)¹. As this star orbits around Cyg OB2 #5 A, the resulting WCR (hereafter WCR(A-B)) is undetected around what is presumed to be orbit periastron, yet can be

¹Kennedy et al. (2010) refer to Cyg OB2 #5 Aa, Ab, B and C as Star A, B, C and D, respectively.

detected as the orbit progresses to apastron. Ortiz–León et al. (2011) noticed that the separation between the WCR(A-B) and the position of the contact binary is 12 mas, i.e. smaller than the nominal radius (23 ± 12 mas; Rodríguez et al. 2010) of the region where the optically–thick free–free radiation of the Cyg OB2 #5 A binary system is produced. Therefore, the WCR(A-B) emission should in principle be undetectable due to the free–free opacity. To resolve this conundrum, these authors proposed that the wind driven by the Cyg OB2 #5 is very inhomogeneous, as suggested for other early massive stars (Blomme et al. 2010; Muijres et al. 2011). However, the time variability could be due to other plasma effects (Pittard & Dougherty 2006; Pittard 2009).

Being part of the Cyg OB2 region, Cyg OB2 #5 is expected to be located at the same distance. Traditionally, the Cyg OB2 region has been believed to be at a distance of 2.1 kpc (Reddish et al. 1966), although it has, more recently, been argued to be somewhat nearer (at about 1.7 kpc; e.g. Massey & Thompson 1991). Even shorter distances have been proposed. For instance, Hanson (2003) suggested $d \sim 1.4$ kpc or even less. Direct trigonometric parallaxes were obtained recently by Rygl et al. (2012) who measured the distances to several methanol and water maser related to objects in the Cygnus X star forming complex. They found that most of them are consistent with a distance of 1.40 ± 0.08 kpc, and suggest that the Cyg OB2 region is located at a similar distance. Using similar techniques, Zhang et al. (2012) measured the distance to the red hypergiant NML Cyg to be 1.61 ± 0.12 kpc and suggested that it lies on the far side of the Cyg OB2 region. Thus, most recent, reliable measurements suggest a distance of 1.4 kpc for the Cyg OB2 region as a whole, and for Cyg OB2 #5 in particular. Interestingly, however, Linder et al. (2009) obtained a distance estimate for Cyg OB2 #5 itself of 925 ± 25 pc from a light curve analysis. A direct astrometric study to Cyg OB2 #5 could help solve the discrepancy between the distance suggested by Linder et al. (2009) and the recently measured distances for other objects in the region.

In this paper, we present the analysis of a series of 12 VLBA observations of the WCR(A-B) in Cyg OB2 #5, covering a total time span of 1.6 years. These data will be used to study the nature of the emission mechanism in the WCR(A-B), and the distance to Cyg OB2 #5. In the past, our team has successfully used multi-epoch VLBA observations to measure distances to low and intermediate mass stars with compact nonthermal radio emission (see Dzib et al. 2010 and 2011 for recent results). In the case of Cyg OB2 #5 the wind collision region is resolved with VLBA observations, but should still be sufficiently compact to enable usable astrometry. A description of the observations, their calibration and imaging are described in Section 2. The results are presented in Section 3, where we also describe the structure and variability of the emission. Additionally a rough estimation of the trigonometric parallax is also presented in this section. The discussion of the results is presented in Section 4, and we finish with the conclusions in Section 5.

2. Observation and data calibration

Cyg OB2 #5 was observed at $\lambda = 3.6$ cm ($\nu = 8.42$ GHz) with the VLBA at 12 epochs between 2010 December and 2012 July. The first observation (in 2010 December) was designed as a detection experiment and was reported by Ortiz-León et al. (2011). Following this successful detection, we initiated a series of multi-epoch observations. The separation between successive observations in those multi-epoch data was about 1.5 months (Table 1). They were usually realized at a recording rate of 512 Mbps but the epoch 2011 October was recorded using a rate of 2 Gbps, to test new VLBA equipment. As a consequence, the noise level for this epoch was significantly better.

The observations consisted of series of cycles with two minutes spent on source, and one minute spent on the main phase-referencing quasar J0218+3851, located $3^{\circ}6'$ away. Every 15 minutes, the radio bright X-ray binary Cyg X-3, located at $20'$ from Cyg OB2

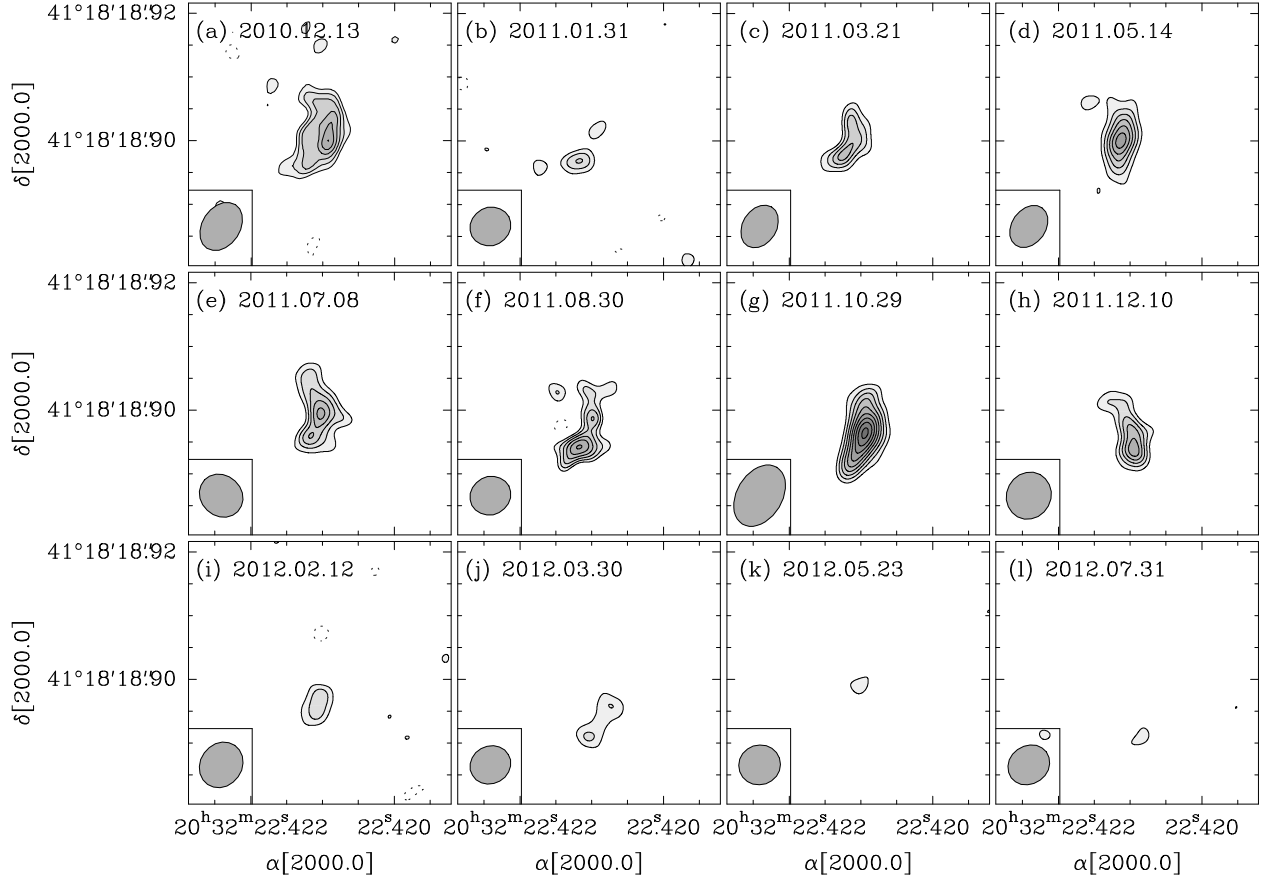


Fig. 1.— Images of Cyg OB2 #5 obtained with the VLBA. The contours are at $-3, 3, 4.5, 6, 7.5, 9$ etc. times the 3σ noise level in the image (see Table 1). The synthesized beam is shown at the bottom left.

#5, was also observed. Although Cyg X-3 is very close to Cyg OB2 #5 it was not used as a primary calibrator due to its extreme variability in both flux density and morphology and the fact it is heavily scattered at the observing frequency (Desai & Fey 2001). As we shall see, however, it was used for secondary calibration. The total duration of the observations was 5 hours for the 2010 December observation and 2 hours for the other epochs.

The data were edited and calibrated using the AIPS software, following standard procedures for phase-referenced VLBA observations. The calibration determined from

the observations of J0218+3851 was applied to both Cyg OB2 #5 and Cyg X-3. At this point, most of the phase errors left are caused by the 3.6 separation between the source and the phase calibrator. To remove most of this, Cyg X-3 was self-calibrated in phase and the incremental phase gains determined from that self-calibration were interpolated and applied to Cyg OB2 #5. In most of the epochs, this resulted in a significant improvement in the quality of the image of Cyg OB2 #5 compared to a direct phase transfer between J0218+3851 and Cyg OB2 #5. For epochs 2011 August and 2011 December, however, this step worsened the image, presumably because of the high variability of Cyg X-3. For those epochs, we use the images obtained without applying this step. Cyg OB2 #5 is quite resolved, so the best images were made by limiting the maximum uv length to 60000 k λ and using always natural weighting. The total flux for each detection in these images was determined using the AIPS task IMSTAT. The rms noise level in the final images (shown in Figure 1) was 43–110 $\mu\text{Jy beam}^{-1}$ (Table 1). Additionally, high resolution images were made using the whole uv range. The epochs at which the source was significantly detected in this second set of images are shown in Figure 2.

As we will see, significant variations in the flux of Cyg OB2#5 were found. It is, therefore, worthwhile to examine in some detail the accuracy of the absolute flux calibration. We followed the standard VLBA recipes, based on gain and system temperature, for the absolute flux calibration. These methods are applied similarly to the target (Cyg OB2 #5) and the gain calibrator (J0218+3851) so any systematic error should affect equally both sources. We inspected the obtained flux of J0218+3851 and found no systematic differences from epoch to epoch. Instead, we found a random scatter of about 0.035 Jy around a mean value of 0.308 Jy. Thus, the dispersion is about 10% of the mean and we will use that figure as our flux uncertainty.²

²Note that J2018+3851 is likely to be intrinsically moderately variable, and part of the

Given the 3.6° separation between the gain calibrator and the target, part of the target flux might be lost under adverse weather conditions due to decorrelation. This can also be discarded using the observations of Cyg X-3 that were intertwined with the observations of Cyg OB2 #5. Cyg X-3 and Cyg OB2 #5 are very near each other (separation of about 0.3°) while the phase calibrator is 3.6° degrees away. Thus, if the phase transfer from the phase calibrator to the target were responsible for significant decorrelation on Cyg OB2#5, it should also induce significant decorrelation on Cyg X-3. We checked that this was not the case in any of our images, by comparing the flux measured in our VLBA observations with (publicly available) monitoring observations of Cyg X-3 made with the AMI-large array telescope at 15 GHz.³

3. Results

3.1. Structure and properties of the emission

From Figure 1 we can see that when the source is detected, the structure is similar to that reported by Ortiz-León et al. (2011): an arc-like morphology, with apex located to the west, extended mostly along the north-south direction. Following Ortiz-León et al. (2011), we attribute this morphology to the interaction between the strong wind driven by the contact binary Cyg OB2 #5 A located about 12 mas to the west of the WCR(A-B) (see Figure 2 in Ortiz-León et al. 2011), and the wind driven by an unseen companion (Cyg OB2

observed scatter might reflect this intrinsic variability. As a consequence, our accuracy might well be better than the quoted 10%.

³ The AMI-large array telescope is supported by STFC and the University of Cambridge and their monitoring can be accessed by the URL <http://www.mrao.cam.ac.uk/telescopes/ami/index.html>.

Table 1: Observed epochs, flux densities (with statistic and systematic errors), and noise levels of the low resolution VLBA Images.

Mean UT date (yyyy.mm.dd)	Modified Julian Day	$f_\nu \pm \sigma_{stat} \pm \sigma_{syst}$ (mJy)	σ ($\mu\text{Jy beam}^{-1}$)
2010.12.13	55543.90	$3.00 \pm 0.13 \pm 0.30$	55
2011.01.31	55592.85	$0.66 \pm 0.10 \pm 0.07$	80
2011.03.21	55641.72	$2.98 \pm 0.18 \pm 0.30$	89
2011.05.14	55695.57	$3.51 \pm 0.16 \pm 0.35$	86
2011.07.08	55750.42	$3.24 \pm 0.16 \pm 0.32$	76
2011.08.30	55803.28	$2.57 \pm 0.13 \pm 0.26$	72
2011.10.29	55863.11	$1.66 \pm 0.07 \pm 0.17$	43
2011.12.10	55906.00	$2.58 \pm 0.13 \pm 0.26$	68
2012.02.12	55969.82	$1.33 \pm 0.16 \pm 0.13$	110
2012.03.30	56016.69	$0.98 \pm 0.14 \pm 0.10$	70
2012.05.23	56070.55	< 0.24	80
2012.07.31	56139.36	< 0.25	84

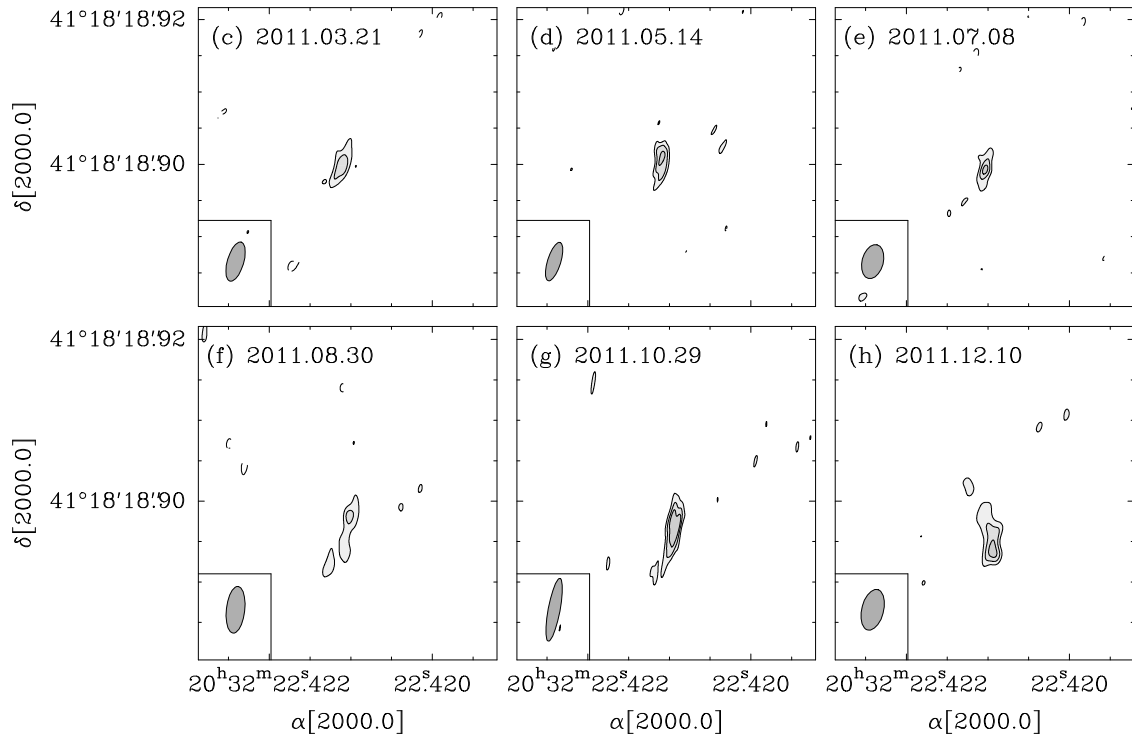


Fig. 2.— Images at higher resolution for the epochs when Cyg OB2 #5 is still detected. The contours are at $-3, 3, 4.5, 6, 7.5, 9$ etc. times the 3σ noise level in the image (see Table 2). The synthesized beam is shown at the bottom left.

#5 B) located just east of the apex (see again Figure 2 in Ortiz–León et al. 2011). This is also the preferred scenario of Kennedy et al. (2010) to explain the VLA observations of the system. In the high resolution images (Figure 2), most of the flux is resolved out, and only the most compact radio emission remains detectable. The implied brightness temperature in these cases is in the range of $0.5\text{--}1.5 \times 10^7$ K (Table 2).

The existing VLA observations of Cyg OB2 #5 imply that the average flux from the WCR(A-B) during high state should be ~ 4.0 mJy at 8.4 GHz (as compared to the total flux of the stellar winds plus WCR(A-B) of ~ 9 mJy; Kennedy et al. 2010). Interestingly, however, the fluxes observed for WCR(A-B) in the VLBA observations reported here (Table 1) are significantly below the value of ~ 4.0 mJy (~ 3 mJy on average). This could be

taken to indicate that the flux in the current “on” state is systematically lower than the previous “on” states. To check this, we searched the archive of the Very Large Array (VLA) for recent observations of the system. We found an observation of the project 12B–165 taken in 2010 August in C band and D configuration. The source was detected at 9.89 ± 0.38 mJy, consistent with previous detection at the same band in the same configuration in previous “on” states (see Kennedy et al. 2010). We suggest, instead, that about 25% of the emission is resolved out by the VLBA.

In Figure 3 the fluxes from Table 1 are plotted as a function of time. From December 2010 to December 2011, the flux is roughly constant at about 3 mJy, except for the observation of 2011 January. After December 2011, the flux starts to decrease, and the source is finally not detected in 2012 May and 2012 July. This flux behavior is consistent with that expected from previous observations of Cyg OB2 #5, and *qualitatively* in agreement with the best formal model (i.e. $s=0$) of Kennedy et al. (2010). Quantitatively, however, the best model of Kennedy et al. (2010) predicted the flux to drop about 7.5 months later than it actually did (see Figure 3).

3.2. Astrometry

For astrometric studies, point-like objects are preferred, and the WCR(A-B) in Cyg OB2 #5 is clearly not the ideal type of target. However, the six high-resolution images shown in Figure 2 can be used to perform some astrometry, albeit with less accuracy than would be achievable for very compact sources. In particular, the extension of the source in declination induces large positional errors along that direction. Although it does include two successive epochs of maximum parallactic elongation (March and September), the total time span covered by our observations is only 8.8 months, and is also not optimal. Bearing in mind these limitations, we attempted an astrometric study of the WCR(A-B) in Cyg

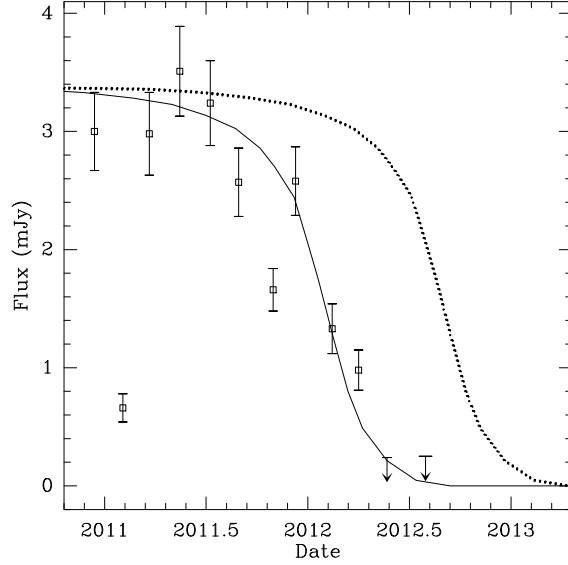


Fig. 3.— Time evolution of the total flux of the WCR(A-B) in Cyg OB2#5, from the low resolution VLBA images. The upper limits are at 3σ . The dotted curve shows the expectation from the best fit of Kennedy et al. (2010; the $s=0$ model) scaled by 0.75 to account for the missing flux (see text), while the solid curve shows the same fit offset by 7.5 months.

OB2 #5.

Table 2: Calendar dates and their corresponding Julian days, measured source positions, flux densities, noise levels, and brightness temperatures of the high resolution VLBA images.

Mean UT date (yyyy.mm.dd/hh:mm)	Julian Day	α (J2000.0) $20^{\text{h}}32^{\text{m}}$	σ_{α}	δ (J2000.0) $+41^{\circ}18'$	σ_{δ}	f_{ν} (mJy)	σ ($\mu\text{Jy beam}^{-1}$)	T_b (10^7 K)
2011.03.21/17:17	2455642.22	$22^{\text{s}}421114$	$0^{\text{s}}000018$	$18^{\text{m}}89983$	$0^{\text{m}}00042$	2.17 ± 0.43	82	1.24
2011.05.14/13:44	2455696.07	$22^{\text{s}}421094$	$0^{\text{s}}000012$	$18^{\text{m}}90079$	$0^{\text{m}}00039$	2.57 ± 0.42	75	1.55
2011.07.08/10:08	2455750.92	$22^{\text{s}}421036$	$0^{\text{s}}000013$	$18^{\text{m}}89937$	$0^{\text{m}}00034$	1.32 ± 0.27	76	0.56
2011.08.30/06:40	2455803.78	$22^{\text{s}}420999$	$0^{\text{s}}000018$	$18^{\text{m}}89792$	$0^{\text{m}}00046$	1.37 ± 0.32	81	1.02
2011.10.29/02:44	2455863.61	$22^{\text{s}}420940$	$0^{\text{s}}000012$	$18^{\text{m}}89689$	$0^{\text{m}}00042$	1.40 ± 0.22	41	0.74
2011.12.10/23:55	2455906.50	$22^{\text{s}}420949$	$0^{\text{s}}000015$	$18^{\text{m}}89466$	$0^{\text{m}}00050$	2.19 ± 0.44	68	0.89

The positions of the source in our VLBA data were determined from the high resolution images shown in Figure 2 using a two-dimensional Gaussian fitting procedure (task JMFIT in AIPS) and are given in Table 2. JMFIT provides an estimate of the position error based on the expected theoretical astrometric precision of an interferometer (Condon 1997); these errors are quoted in Columns 4 and 6 of Table 2. To obtain the astrometric parameters from these data, we used the single value decomposition fitting scheme described by Loinard et al. (2007). The necessary barycentric coordinates of the Earth, as well as the Julian date of each observation, were calculated using the Multi-year Interactive Computer Almanac (MICA) distributed as a CD ROM by the US Naval Observatory. The reference epoch was taken at the mean of the four observations: JD 2455774 \equiv 2011.6. The best fit is shown in Figure 4, and yields the following astrometric elements:

$$\begin{aligned}\alpha_{J2011.6} &= 20^{\text{h}}32^{\text{m}}22^{\text{s}}.421021 \pm 0.000006 \\ \delta_{J2011.6} &= 41^{\circ}18'18''.89823 \pm 0.00032 \\ \mu_{\alpha} \cos \delta &= -1.64 \pm 0.98 \text{ mas yr}^{-1} \\ \mu_{\delta} &= -7.16 \pm 1.28 \text{ mas yr}^{-1} \\ \pi &= 0.61 \pm 0.22 \text{ mas},\end{aligned}$$

corresponding to a distance of $1.65_{-0.44}^{+0.96}$ kpc. This is in agreement with the recent distances measured for sources related with the Cygnus-X complex (Zhang et al. 2012; Rygl et al. 2012) and significantly larger than the value obtained by Linder et al. (2009) for Cyg OB2 #5 itself. The post-fit rms in this case is 0.13 mas in right ascension and 0.55 mas in declination. The reduced- χ^2 obtained in right ascension using the errors delivered by JMFIT is 0.59, suggesting that no significant systematic errors remain in our data along that axis. In declination, however, a systematic contribution of 0.65 mas has to be added quadratically to the errors given by JMFIT to obtain a reduced- χ^2 of 1. This is not

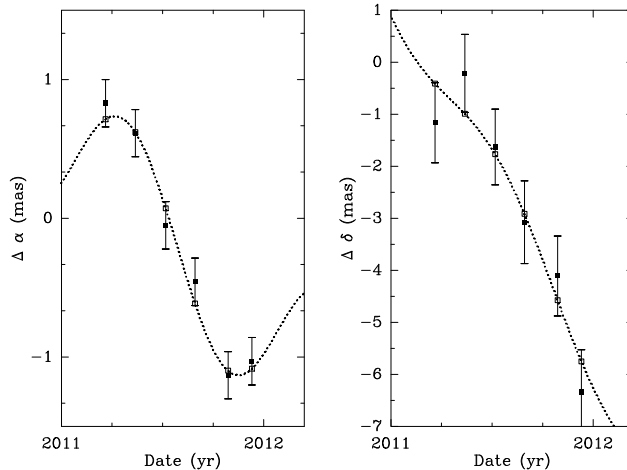


Fig. 4.— Best astrometric fit to the positions obtained from the high resolution VLBA images. The left panel shows the right ascension as a function of time, while the right panel shows the declination behaviour. The filled squares show the observed positions with their error bars (including the systematic contributions) while the open squares indicate the position of the source expected from the fits at each epoch. The dotted curves are the best fits to the data including a parallax and uniform proper motion.

surprising given the elongation of the source in the north-south direction. All the errors quoted here include this systematic contribution.

4. Discussion

4.1. Nature of the radio emission from the WCR(A-B)

The emission from the WCR(A-B) has long been thought to be of non-thermal origin because (i) the flat radio spectrum of Cyg OB #5 in VLA observations when this source is “on” compared to its positive spectral index when it is “off” suggests that the spectral index of the WCR(A-B) is negative, and (ii) Ortiz-León et al. (2011) measured a brightness temperature of $\sim 2 \times 10^6$ K suggestive of a non-thermal process. The brightness

temperatures reported here are about 10^7 K, clearly favoring a non-thermal (presumably synchrotron) nature.

The best-fit model of Kennedy et al. (2010) has orbital parameters (orbit inclination $i = 90^\circ \pm 40^\circ$, argument of periastron $\omega = 319^\circ \pm 3^\circ$ and eccentricity $e = 0.7 \pm 0.04$) that result in a structure as shown in Figure 5 (the plot is made in the plane of the orbit, perpendicular to the plane of the sky). The large circle shows the nominal size (radius 23 mas) of the free-free emission region from the Cyg OB2 #5 A contact binary together with its uncertainty (12 mas; Rodríguez et al. 2010). It is clear that near apastron (and only near apastron), Cyg OB2 #5 B (and its associated WCR(A-B)) are located outside, or at least near the outer edge, of the optically-thick ionized region. This occurs because the orbit is quite eccentric, and explain why the non-thermal emission is detectable in spite of the small separation between the WCR(A-B) and the contact binary. Note that since Cyg OB2 #5 B will always be located **to the east** of Cyg OB2 #5 A at apastron, the curvature of the WCR(A-B) is expected to always be oriented in nearly exactly the same direction, as observed in our VLBA data. On the other hand, we note that the decline in flux of the WCR(A-B) around periastron can be influenced by other plasma and radiation processes (Pittard & Dougherty 2006; Pittard 2009).

As we mentioned before, the flux of the WCR(A-B) is consistent with a value of 3 mJy from 2010 December to 2011 December. There is, however, one exception: the flux in 2011 January is nearly 5 times smaller than this average value. Our discussion of the absolute flux accuracy (end of Section 2) shows that our fluxes are accurate to about 10% so the decrease by a factor of 5 observed at that epoch cannot be ascribed to instrumental effects. Such strong variability is not expected in a wind collision region. The $s=0$ model of Kennedy et al. (2010) predicts that the flux of the WCR(A-B) is closely constant in the "on" state. A possible solution to this discrepancy would be for the wind driven by

the contact binary to be inhomogeneous. Under this assumption, two scenarios would be possible. The first one would be for Cyg OB2 #5 B to pass through a region where the wind driven by Cyg OB2 #5 A is less dense. In such a situation, the shock resulting from the wind collision might be weak, and insufficient to produce relativistic electrons and, therefore, detectable compact radio emission. Araudo et al. (2012, in preparation) computed the cooling time for the relativistic electrons at the WCR(A-B) considering synchrotron losses, Inverse Compton (IC) scattering, relativistic bremsstrahlung, and advection and diffusion escape of the relativistic particles from the shocked winds. They found that due to the dense photon stellar field provided by the unseen companion, IC scattering is the most important cooling channel for the relativistic electrons at energies above $\sim 10^6$ eV (considering different spectral types for Cyg OB2 #5 B), implying that most of the relativistic electrons are cooled by IC losses. Below this energy, the cooling is dominated by advection of the particles on a time $t_{\text{esc}} \sim 4l_{\text{bs}}/v_{\infty} \sim 4$ months. Here l_{bs} is the size of the WCR(A-B) and v_{∞} the terminal velocity of the stellar winds. Since the separation between our successive observations is significantly shorter than this, we would not expect the flux to drop appreciably between observations. A second way to produce a drop in radio flux would be to have a sudden increase in the column density of ionized material along the line of sight to the WCR(A-B), for instance as a result of a dense clump passing in front of the WCR(A-B). This would result in an increase in the free-free opacity. This second scenario fits more naturally the observed light curve.

4.2. The distance to Cyg OB2 #5

As we mentioned in the Introduction, there is some significant uncertainty on the distance to Cyg OB2 #5. On the one hand, recent trigonometric parallax measurements to masers associated with several stars in the Cygnus X star forming complex, including

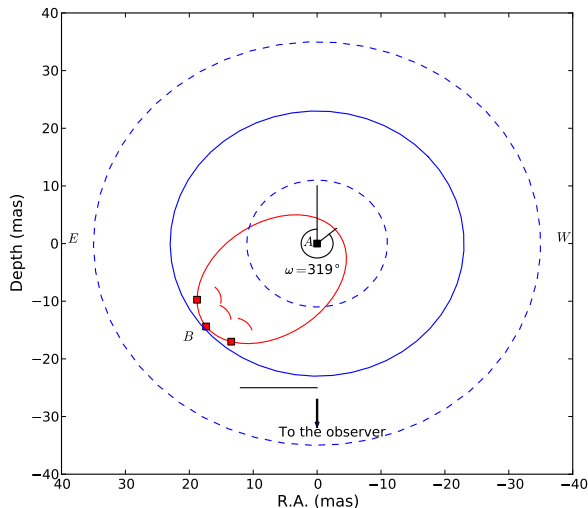


Fig. 5.— Graphical sketch of the orbit Cyg OB2 #5 B (red line). The blue circle shows the extent of the optically–thick photo–ionized region surrounding Cyg OB2 #5 A (the full line is the nominal value, while the dashed versions show the minimum and maximum values; from Rodríguez et al. 2010)). As the sizes depends on the distance assumed, the values of both R.A. and depth are presented here in angular units (mas). The black line is the angular separation observed in the plane of the sky. The red squares shows the position of Cyg OB2 #5 B at three representative epochs when the WCR(A-B) can be detected to show the direction of the curvature of the WCR(A-B) (red arcs) in these epochs.

the Cygnus OB2 star forming region, suggest a distance of 1.4–1.6 kpc (Rygl et al. 2012; Zhang et al. 2012). On the other hand, Linder et al. (2009) obtained a distance modulus for Cygnus OB2 #5 that yields a significantly shorter distance of 925 pc. The latter authors noted that their results were strongly dependent on the assumed stellar effective temperature. The value used was 36,000 K, as obtained from a spectrum analysis carried by Rauw et al. (1999), that suggested an O6–7 Ia star. They also mention that a somewhat unlikely effective temperature of 48000 K would be needed if the system were located to a distance of 1.7 kpc. The parallax obtained here, although uncertain, favors a distance

of order 1.6 kpc, in agreement with those obtained by Rygl et al. (2012) and Zhang et al. (2012) and significantly larger than the distance of 925 pc proposed by Linder et al. (2009)

The distance to the Cyg OB2 #5 system can also be estimated using an orbital parallax method. From our VLBA observations and the argument of periastron (ω) and inclination (i) of the Cyg OB2 #5 AB orbits derived by Kennedy et al. (2010), we can derive the de-projected angular separation between Cyg OB2 # 5 A and Cyg OB2 # 5 B. In all four models discussed by Kennedy et al. (2010) the inclination is close to 90° (in the range of 85° to 90°) and can be ignored in the derivation. Then, the de-projected angular distance is simply equal to the projected angular distance divided by $\sin(360^\circ-\omega)$. For the case of the best fit model $s=0$, we find that at apastron the de-projected angular distance is 18.3 mas^4 . The total mass of Cyg OB2 #5 A was calculated to be $41.5 \pm 3.4 M_\odot$ by Linder et al. (2009) and the mass of Cyg OB2 #5 B was estimated to be $23_{-14}^{+22} M_\odot$ by Kennedy et al. (2010). Thus, the appropriate mass range for the Cyg OB2 #5 AB system is between 50 and $90 M_\odot$. From the orbital parameters given by Kennedy et al. (2010), we can calculate the true separation (in cm) at apastron for these two masses, and from the comparison between the true separation and the de-projected angular separation, deduce the distance to the system. We obtain distances between 1.26 kpc and 1.53 kpc. This is in excellent agreement with the parallax determination obtained earlier, and with the distance to Cyg OB2 estimated by Rygl et al. (2012) and Zhang et al. (2012). We note, on the other hand, that if we assume a distance of 0.95 kpc, the total mass of the triple system would have to be only $21.4 M_\odot$, lower than the primary alone. At the other extreme, assuming a distance of 1.7 kpc would yield a dynamical mass of $122.4 M_\odot$, larger than usually expected.

⁴Strictly, this is the separation between Cyg OB2 # 5 A and the WCR(A-B) associated with Cyg OB2 # 5 B, but Ortiz-León et al. (2011) argue that Cyg OB2 #5B is very near the apex of the WCR(A-B).

Unfortunately, this method depends critically on the orbital parameters, and adoption of any other models in Kennedy et al. (2010) will give a different distance.

Yet another (independent) distance determination can be obtained as follows. The separation between Cyg OB2 #5 B and the WCR(A-B) can be estimated from a momentum ratio analysis. From Cantó et al. (1996), we can relate the separation R_0 between Cyg OB2 #5 B and the WCR(A-B) to the separation R_1 between the WCR(A-B) and Cyg OB2 #5 A by:

$$R_0 = \eta^{1/2} R_1, \quad (1)$$

where $\eta = \dot{M}_{w0}V_{w0}/\dot{M}_{w1}V_{w1}$ is the ratio between the wind momentum ratio of the two stars. Linder et al. (2009) suggest a distance-independent mass loss rate of $\sim 2.1 \times 10^{-5} M_{\odot} \text{ year}^{-1}$ for Cyg OB2 #5 A. Its terminal velocity was suggested to be 1500 km s^{-1} by Kennedy et al. (2010) based on the absorption of the P-Cygni HeI $1.083 \mu\text{m}$ line observed by Linder et al. (2009).

The value of η will, of course, depend on the mass-loss rate and wind velocity of Cyg OB2 #5 B. In Table 3 we summarize the parameters of massive stars with luminosity class V. The effective temperature, luminosity, radius, spectroscopic mass, and the flux of ionizing photons are taken from Vacca et al. (1996). The mass loss rate was calculated following the prescription of Vink et al. (2001) for stars of solar metallicity, and the terminal velocity of the wind, v_{∞} , was calculated assuming $v_{\infty}/v_{\text{esc}} = 2.6$ (Vink et al. 2000), where v_{esc} is the escape velocity from the stellar surface. Finally, we calculated the expected flux density at 8.46 GHz assuming a fully ionized, pure hydrogen wind at a distance of 1 kpc and following the formulation of Panagia & Felli (1975). We also used Equation 1 of Rodríguez & Cantó (1983) to verify that the ionizing photon rate of the stars was sufficient to fully ionize their respective winds.

Table 3: Parameters of massive stars with luminosity class V. The 4.8 GHz flux is estimated for a distance of 1 kpc. Additionally, the value of η for each type of star is listed in the rightmost column, assuming that its wind would interact with that of Cyg OB2 #5 A.

Spectral Type	T_{eff} (K)	$\log(L/L_{\odot})$	$\log(R/R_{\odot})$	$\log(M/M_{\odot})$	$\log(N_i)$	$\log(\dot{M})$ ($M_{\odot} \text{ year}^{-1}$)	v_{∞} (km s^{-1})	$S_{8.46\text{GHz}}$ (mJy)	η
O3	51230	6.035	1.12	1.71	49.87	-4.90	3200	1.335	1.270
O4	48670	5.882	1.09	1.65	49.70	-5.13	3100	0.687	0.730
O4.5	47400	5.805	1.07	1.61	49.61	-5.24	3000	0.512	0.540
O5	46120	5.727	1.06	1.58	49.53	-5.36	2900	0.371	0.411
O5.5	44840	5.647	1.04	1.55	49.43	-5.49	2900	0.249	0.298
O6	43560	5.567	1.03	1.52	49.34	-5.63	2800	0.169	0.210
O6.5	42280	5.486	1.01	1.49	49.23	-5.77	2800	0.110	0.152
O7	41010	5.404	1.00	1.46	49.12	-5.92	2700	0.073	0.102
O7.5	39730	5.320	0.98	1.43	49.00	-6.08	2700	0.044	0.070
O8	38450	5.235	0.97	1.40	48.87	-6.24	2600	0.029	0.048
O8.5	37170	5.149	0.95	1.37	48.72	-6.41	2600	0.017	0.032
O9	35900	5.061	0.94	1.35	48.56	-6.61	2600	0.009	0.020
O9.5	34620	4.972	0.93	1.32	48.38	-6.79	2500	0.006	0.013
B0	33340	4.881	0.92	1.29	48.16	-6.99	2500	0.003	0.008
B0.5	32060	4.789	0.90	1.26	47.90	-7.21	2400	0.002	0.004

Cyg OB2 #5 B must drive a wind strong enough to produce the WCR(A-B) when it interacts with the winds of the eclipsing binary Cyg OB2 #5 A. As discussed by Kennedy et al. (2010) and Ortiz-León et al. (2011), this suggests that Cyg OB2 #5 B is of B0.5 or earlier spectral type. The value of η for a B0.5 star (Table 3) yields an upper limit on the distance to Cyg OB2 #5 of 1.44 kpc. This result is, again, in agreement with our measured trigonometric parallax, and with distances proposed by Hanson (2003), Rygl et al. (2012) and Zhang et al. (2012).

Running the same argument in reverse, we can place an upper limit on the value of η considering the highest possible mass for the system ($90 M_{\odot}$) and shortest possible distance (1.26 kpc). This leads to $\eta = 0.047$, corresponding to a spectral type O8 for Cyg OB2 #5 B. This explains *a posteriori* why Cyg OB2 #5 B contributed negligibly to the thermal radio emission of the system: the total free-free emission from an O8 star at the distance of Cyg OB2 #5 being only about $30 \mu\text{Jy}$.

It is important to keep in mind that our results depend strongly on the orbital parameters reported by Kennedy et al. (2010). Fortunately, once a model is selected, their largest errors are in the inclination of the orbit, while our calculations depend most strongly on the argument of periastron and the eccentricity.

5. Conclusions

In this paper, we presented an analysis of a series of multi-epoch VLBA observations of the compact wind collision region in the Cygnus OB2 #5 quadruple system. The brightness temperatures for the most compact emission is $\sim 10^7$ K, clearly suggestive of a non-thermal process. The total measured flux is consistent with a constant value of ~ 3 mJy for the first seven epochs, but falls below the detection limit for the latest observations. This is

consistent with the interpretation proposed by Kennedy et al. (2010) that the shocked region plunges into the photo-ionized region surrounding the primary in the system. In addition, in one of the early epochs, the flux drops significantly. We suggest that for this epoch, a dense clump of the inhomogeneous wind intersect the sight of view, and the free-free emission partially hides the non-thermal emission from the wind collision region.

The measured trigonometric parallax for the system corresponds to a distance of $1.65_{-0.44}^{+0.96}$ kpc. In addition, the distance to the system was estimated using two indirect methods, both yielding distances of order 1.3–1.4 kpc. These results are in agreement with recently measured trigonometrical parallaxes to masers related with objects in the Cygnus X star forming complex, and discard the small value of 950 pc suggested by Linder et al. (2009).

A new set of VLBA observations when the WCR(A-B) comes back to its "on" state, combined with the positions presented in this work, could be used for a better determination of the trigonometrical parallax of the Cygnus OB2 #5 quadruple system. We note that in agreement with Kennedy et al. (2010) the next "on" state will be on 2014 summer.

S.A.D., L.F.R., L.L., G.O.L. and A.T.A. acknowledge the financial support of DGAPA, UNAM and CONACyT, México. L.L. is indebted to the Alexander von Humboldt Stiftung for financial support. The National Radio Astronomy Observatory is a facility of the National Science Foundation operated under cooperative agreement by Associated Universities, Inc.

REFERENCES

- Araudo, A. T., Ortiz–León, G. N., & Rodríguez, L. F. 2012, in preparation
- Blomme, R., De Becker, M., Volpi, D., & Rauw, G. 2010, *A&A*, 519, A111
- Cantó, J., Raga, A. C., & Wilkin, F. P. 1996, *ApJ*, 469, 729
- Condon, J. J. 1997, *PASP*, 109, 166
- Contreras, M. E., Rodríguez, L. F., Tapia, M., Cardini, D., Emanuele, A., Badiali, M., & Persi, P. 1997, *ApJ*, 488, L153
- De Becker, M. 2007, *A&A Rev.*, 14, 171
- Desai, K. M., & Fey, A. L. 2001, *ApJS*, 133, 395
- Dzib, S., Loinard, L., Mioduszewski, A. J., Boden, A. F., Rodríguez, L. F., & Torres, R. M. 2010, *ApJ*, 718, 610
- Dzib, S., Loinard, L., Rodríguez, L. F., Mioduszewski, A. J., & Torres, R. M. 2011, *ApJ*, 733, 71
- Hanson, M. M. 2003, *ApJ*, 597, 957
- Herbig, G. H. 1967, *PASP*, 79, 502
- Kennedy, M., Dougherty, S. M., Fink, A., & Williams, P. M. 2010, *ApJ*, 709, 632
- Linder, N., Rauw, G., Manfroid, J., Damerdji, Y., De Becker, M., Eenens, P., Royer, P., & Vreux, J.-M. 2009, *A&A*, 495, 231
- Loinard, L., Torres, R. M., Mioduszewski, A. J., Rodríguez, L. F., González-Lópezlira, R. A., Lachaume, R., Vázquez, V., & González, E. 2007, *ApJ*, 671, 546

- Massey, P., & Thompson, A. B. 1991, *AJ*, 101, 1408
- Muijres, L. E., de Koter, A., Vink, J. S., et al. 2011, *A&A*, 526, A32
- Ortíz-León, G. N., Loinard, L., Rodríguez, L. F., Mioduszewski, A. J., & Dzib, S. A. 2011, *ApJ*, 737, 30
- Panagia, N., & Felli, M. 1975, *A&A*, 39, 1
- Pittard, J. M. 2009, *MNRAS*, 396, 1743
- Pittard, J. M., & Dougherty, S. M. 2006, *MNRAS*, 372, 801
- Rauw, G., Vreux, J.-M., & Bohannan, B. 1999, *ApJ*, 517, 416
- Reddish, V. C., Lawrence, L. C., & Pratt, N. M. 1966, *Publications of the Royal Observatory of Edinburgh*, 5, 111
- Rodríguez, L. F., & Canto, J. 1983, *Rev. Mexicana Astron. Astrofis.*, 8, 163
- Rodríguez, L. F., Gómez, Y, Loinard, L., & Mioduszewski, A. J. 2010, *RMxAA*, 46, 215
- Rygl, K. L. J., Brunthaler, A., Sanna, A., et al. 2012, *A&A*, 539, A79
- Vacca, W. D., Garmany, C. D., & Shull, J. M. 1996, *ApJ*, 460, 914
- Vink, J. S., de Koter, A., & Lamers, H. J. G. L. M. 2000, *A&A*, 362, 295
- Vink, J. S., de Koter, A., & Lamers, H. J. G. L. M. 2001, *A&A*, 369, 574
- Zhang, B., Reid, M. J., Menten, K. M., Zheng, X. W., & Brunthaler, A. 2012, *A&A*, 544, A42